Energetics of Mg and B adsorption on polar zinc oxide surfaces from first principles

Kazume Nishidate,* Masahito Yoshizawa, and Masayuki Hasegawa
Faculty of Engineering, Iwate University, Morioka 020-8551, Japan
(Received 26 July 2007; revised manuscript received 18 October 2007; published 28 January 2008)

We have performed first-principles density-functional projector augmented-wave calculations to investigate the energetics of Mg and B adsorption on polar zinc oxide (ZnO) surfaces, thereby to understand the origin of the peculiar affinities between an epitaxial MgB_2 film and the ZnO substrate. We found that the (0001) Zn surface is relatively inert, while the $(000\bar{1})$ O surface is very reactive in the adsorption of atomic species, where a triplaner BO_3 (a hump of MgO_3) binding unit is formed as a consequence of the B (Mg) atom adsorption on the surface. These binding units would be formed at an early stage in the epitaxial growth of MgB_2 film on the ZnO substrate, and subsequently lead to the formation of the reaction products that were recently found in the interface between the MgB_2 film and the ZnO substrate.

DOI: 10.1103/PhysRevB.77.035330 PACS number(s): 73.20.Hb, 71.20.Nr, 71.55.Gs, 71.15.Mb

I. INTRODUCTION

The discovery of the superconductivity at a transition temperature (T_c) of 39 K in magnesium diboride[1] (MgB_2) has attracted much attention for its scientific implications as well as technological applications. To fabricate MgB_2-based superconductor devices, it is very important to use a high-quality as-grown film prepared at low temperatures. An as-grown process without postannealing is desirable for developing devices such as tunneling junctions and multilayer structure of MgB_2. Several groups have reported low-temperature growth of MgB_2 films on the Al_2O_3 (0001) or Si (111) substrates using molecular beam epitaxy (MBE),[2–4] electron-beam evaporation,[5] pulsed laser deposition,[6] and sputtering.[7] However, these substrates have rather large lattice mismatch with MgB_2 ($\delta \simeq 20\%$), which is unfavorable for the epitaxial growth. It has been reported that the use of in-plane-lattice buffer layers with little mismatch, such as AlN ($\delta \simeq 1.9\%$) and TiZr ($\delta \simeq 3.6\%$), with Al_2O_3 (0001) substrate could improve the crystallinity of MgB_2.[8,9] The T_c values of MgB_2 on the AlN and TiZr buffer layers were 29.8 and 35.1 K, respectively. These results indicate the importance of minimizing lattice mismatch between layers. Recently, as-grown MgB_2 thin films in an ultrahigh vacuum MBE cell have been fabricated under the conditions of low temperature and low growth rate.[10] In these fabrications, several substrates such as MgO, ZnO, Al_2O_3, $SrTiO_3$, and Si have been explored to further refine the crystallinity of MgB_2 films. Among these substrates, ZnO has been thought to be the best as its lattice constant, $a=3.351$ Å, is very close to that of the MgB_2, $a=3.083$ Å, and both have the same hexagonal lattice symmetry. In fact, c-axis oriented MgB_2 film with $T_c=35.0$ K on the polar ZnO substrate has been successfully fabricated,[11] but, at the same time, a certain amount of unfavorable reaction products has also been found in the interface between the MgB_2 film and the ZnO substrate.[10] This experimental finding suggests the importance of the *affinities* between substrate and film in addition to minimizing lattice mismatch. Although these reaction products were supposed to be a derivative of the Mg adatom on the ZnO surface, its energetics, as well as the local atomic structure, has not yet been examined. In the present study, we use an *ab initio* method to investigate the energetics of Mg and B adsorption on the ZnO polar surfaces, thereby to understand the origin of the peculiar affinities between the epitaxial MgB_2 film and the ZnO substrate.

II. COMPUTATIONAL DETAILS

A. Structural parameters of the ZnO crystal

Density-functional electronic structure calculations are performed using the Vienna *ab initio* simulation package (VASP).[12] The total energy is calculated using the projector augmented-wave (PAW) method.[13,14] We first determine the structural parameters of the ZnO crystal to verify the performance of our computational method. For this purpose, we adopt rather stringent computational conditions; the reciprocal space integration is performed with the 20^3 dense Monkhorst-Pack mesh[15] and the high cutoff energy of 500 eV is used in the plane-wave expansion. The exchange-correlation energy functional is treated in the generalized-gradient approximation (GGA) of Perdew *et al.* (GGA-PBE).[16,17] For comparisons, we also adopt the local density approximation[18,19] (LDA) and the GGA of Perdew and Wang (GGA-PW91).[20] The lattice parameters optimized in the LDA are slightly underestimated as compared with the experimental values, while those in the GGA (PW91 and PBE) are slightly overestimated (Table I). A similar trend has

TABLE I. Optimized structural parameters of bulk ZnO and their comparisons with experiments. a and c are the basal and c-axis lattice constants of the wurtzite structure, and u is the internal coordinate which determines the relative position of the Zn and O sublattice along the c axis.

	a (Å)	c (Å)	u
LDA	3.202	5.141	0.3817
PW91	3.288	5.271	0.3817
PBE	3.295	5.282	0.3817
Experimental[a]	3.250	5.207	0.3819

[a]Reference 24.

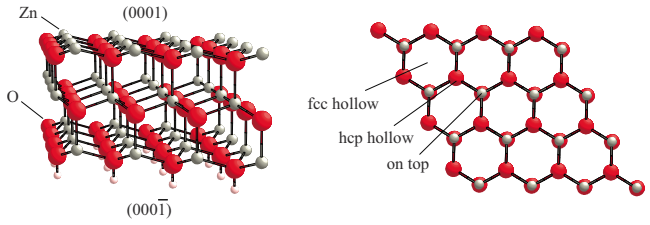

FIG. 1. (Color online) (a) Perspective and (b) top views of (0001) Zn surface slab. The large- and middle-sized spheres are the O and Zn atoms, respectively, and the small spheres below the bottom (000$\bar{1}$) plane are hydrogenlike peseudoatoms introduced to saturate the dangling bonds. The geometry of the (000$\bar{1}$) O surface (not shown here) is obtained by interchanging the atomic species, Zn and O.

also been reported for ZnO crystal[21,22] and for a variety of materials including diatomic molecules.[23] Hereafter, we adopt the GGA-PBE to keep consistency throughout this work.

B. Surface slab

ZnO is a wide-gap semiconductor and expected to be an important material for optoelectronic device applications.[25] It consists of hexagonal Zn and O planes alternatively stacked along the c axis. When the crystal is cleaved in the plane perpendicular to the c axis, the two opposing polar surfaces are different; one is the (0001) Zn surface and the other the (000$\bar{1}$) O surface. We may expect different reactivities for these two surfaces for the adsorption of Mg and B atoms. To investigate adsorption energetics of an isolated atom on the polar ZnO surfaces, we used a large hexagonal slab containing $4\times4\times2$ ZnO unit cells. Kresse *et al.*[22] have suggested that the convergence of total energy calculations with respect to slab thickness can be accelerated by filling (removing) the electron holes (extra electrons) at the O-terminated (Zn-terminated) back side. We achieved convergence by saturating the dangling bonds on the back side of each polar surface; the oxygen (zinc) dangling bonds on the back side of (0001) Zn slab [(000$\bar{1}$) O slab] are terminated by adding pseudoatoms with the valency of $0.5|e|$ ($1.5|e|$) [Fig. 1(a)]. The optimized bond lengths between a saturating pseudoatom and the O and Zn back side atoms are 1.056 and 1.623 Å, respectively. We considered three high-symmetry points as the adsorption sites:[21] "on top" position just above the surface atom, "hcp-hollow" above the atom in the second surface layer, and "fcc hollow" with no atom beneath [Fig. 1(b)]. A large vacuum region over the surface (18.5 Å) is taken to eliminate the interaction between the surfaces. We considered only two k points in the slab calculations and the cutoff energy of 350 eV was used for the plane-wave basis expansion because of the limited computational resources. All the atoms were allowed to relax under the condition that the residual force acting on each atom becomes less than 0.01 eV/Å.

TABLE II. Reference states and their optimized structural parameters used to evaluate the atomic chemical potentials μ_X.

	Reference state		Structural parameter	
	State	Symmetry	Experimental (Å)	Optimized (Å)
Mg	Metal	hcp	$a=3.2093$[a] $c=5.2107$	$a=3.1918$ $c=5.1916$
Zn	Metal	hcp	$a=2.664$[a] $c=4.9494$	$a=2.6570$ $c=4.9343$
B	Metal	Rhombohedral $R\bar{3}m$	$a=5.06$[b] ($\alpha=58°4'$[c])	$a=5.041$ ($\alpha=58°17'$[c])
O	$^3O_2$ molecule[d]		$r=1.208$[e]	$r=1.2330$ (1.2203[e])

[a]Reference 26.
[b]Reference 27.
[c]α is the angle between the crystallographic axes.
[d]Oxygen molecule in the spin triplet state. The atomic chemical potential is raised by ~0.51 eV if we adopt an oxygen molecule in the spin singlet state ($^1O_2$).
[e]Reference 23.

C. Atomic chemical potentials

The adsorption energy of an atom X adsorbed on the site (=fcc, hcp, or top), $\Delta E_{\mathrm{ads}}^{X_{site}}$, is defined here as

$$\Delta E_{\mathrm{ads}}^{X_{site}} = E_{\mathrm{slab}+X_{site}}^{\mathrm{tot}} - E_{\mathrm{slab}}^{\mathrm{tot}} - \mu_X, \tag{1}$$

where $E_{\mathrm{slab}+X_{site}}^{\mathrm{tot}}$ and $E_{\mathrm{slab}}^{\mathrm{tot}}$ are the total energies of the slab with and without an adatom X on the site, respectively. The atomic chemical potentials μ_X of adatoms X_{site} are evaluated separately in their reference states. Here, we define the

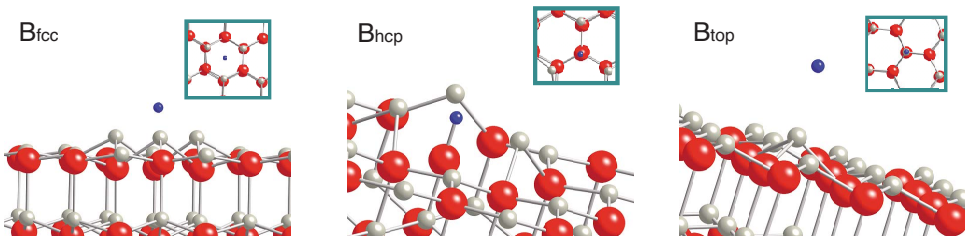

FIG. 2. (Color online) Atomic configuration of the (0001) Zn surface adsorbing a B atom. Top views are also shown in the squares. Large- and middle-sized spheres are the oxygen and zinc atoms, respectively, and the small dark spheres are the B adsorbed on the surface.

TABLE III. Adsorption energies ΔE_{ads} (in unit of eV) and the local geometries of the adatom X_{site} (X=B or Mg) on the site (=fcc, hcp, or top) of the (0001) Zn surface. The numbers (n) and species (spc.) of neighboring atoms within 3 Å from the X=site are tabulated. The distances between the adatom X on the site and the neighboring atoms are indicated in parentheses (in unit of Å).

X_{site}		fcc	hcp	top
B	ΔE_{ads}	1.977	0.889	4.297
	n spc.	3 Zn (2.09)	3 Zn (2.19)	Zn (2.14)
		3 O (2.93)	O (1.31)	⋯
Mg	ΔE_{ads}	0.495	0.474	0.942
	n spc.	2 Zn (2.75)	2 Zn (2.71)	Zn (2.76)
		Zn (2.77)	Zn (2.75)	⋯

atomic chemical potential as a calculated total energy per atom in its optimized reference state.[28] The adsorption energy defined in this way is not the same as the one observed in experiments but may be viewed as a conventional one accounting for the relative stability in the concerned adsorption process. Reciprocal space integrations were performed using the 20^3 Monkhorst-Pack mesh[15] for the bulk metals, and only the Γ point is used for an O_2 molecule placed in a large vacuum supercell with volume of 15^3 Å^3. Converged results were obtained using the cutoff energy of 500 eV for the plane-wave expansion. The reference states and their optimized structural parameters are summarized in Table II.

D. Vacancy formation energies

With the same computational details, we next evaluate the formation energy of a vacancy V_X (X=Zn or O) on the surface defined as

$$\Delta E_f^{V_X} = E_{\text{slab}+V_X}^{\text{tot}} - E_{\text{slab}}^{\text{tot}} + \mu_X, \tag{2}$$

where $E_{\text{slab}+V_X}^{\text{tot}}$ is the total energy of the slab with a vacancy on its surface. The equilibrium constraint for the atomic chemical potential[29] is given by

$$\mu_{\text{ZnO(bulk)}} = \mu_{\text{Zn}} + \mu_{\text{O}} + dh_{\text{ZnO(bulk)}}, \tag{3}$$

where $\mu_{\text{ZnO(bulk)}}$ is the chemical potential of bulk ZnO and customarily obtained as half of the total energy of the ZnO primitive unit cell. With this definition, we obtained enthalpy of formation for the ZnO crystal as $dh_{\text{ZnO(bulk)}}$=−2.903 eV,

TABLE IV. Adsorption energies ΔE_{ads} (in unit of eV) of the adatom X (B or Mg) on the $(000\bar{1})$ O surface. The other details are the same as those in Table III.

		fcc	hcp	top
B	ΔE_{ads}	−5.822	−5.642	−0.115
	n atm. (Å)	3 O (1.40)	O (1.38)	O (1.27)
		3 Zn (2.36)	2 O (1.42)	3 Zn (2.98)
			Zn (2.35)	
Mg	ΔE_{ads}	−4.787	−4.295	−4.789
	n atm. (Å)	3 O (1.97)	3 O (2.00)	3 O (1.97)
		3 Zn (2.67)	Zn (2.35)	3 Zn (2.67)

which is compared to the experimental value of −3.63 eV.[30] By adjusting the atomic chemical potentials in the range μ_X to $\mu_X + dh_{\text{ZnO}}$, we can take into account the Zn-rich and O-rich atmospheric conditions for the defect formations; i.e., in the Zn-rich (O-rich) condition, μ_{Zn} (μ_{O}) is fixed at the value evaluated in its reference state, while μ_{O} (μ_{Zn}) is replaced by $\mu_{\text{O}} + dh_{\text{ZnO}}$ ($\mu_{\text{Zn}} + dh_{\text{ZnO}}$). This procedure, which is simple and rather tractable, has been successfully used in the first-principles calculations to investigate the defect physics of semiconductors.[29,31] Under the oxygen-rich condition, the formation energy of V_{Zn} on the (0001) Zn surface is −3.42 eV if we use the oxygen atomic chemical potential with respect to the oxygen molecule in its triplet state $^3O_2$ (see Table II). If the oxygen molecule in its singlet state $^2O_2$ is adopted as the reference state, that value becomes −2.91 eV, which is compared with the reported theoretical value of −3.11 eV (extrapolated from Fig. 6 of Ref. 22). In the following, we use the μ_{O} obtained in the $^3O_2$ state for consistency. For the oxygen vacancy concentration of 25%, its formation energy per vacancy has been reported to be +1.75 eV for a sixfold (2×2) arrangement of the vacancy, V_{O}(sixfold), and +1.54 eV for a rectangular arrangement of the vacancy, V_{O}(rect).[32] However, we obtained the formation energies of +0.67 eV for the V_{O}(sixfold) and +0.46 eV for the V_{O}(rect), both being about one-third of the previous ones. We cannot trace the origin of these numerical differences in detail but it is possibly ascribed to the difference of the models. In the previous calculations,[32] the back side of the slab was not terminated and the extra energy income of the residual dipole would have contributed to the formation energies even after their own energy corrections. For our slab with only one vacancy (this is for the case with lower V_{O}

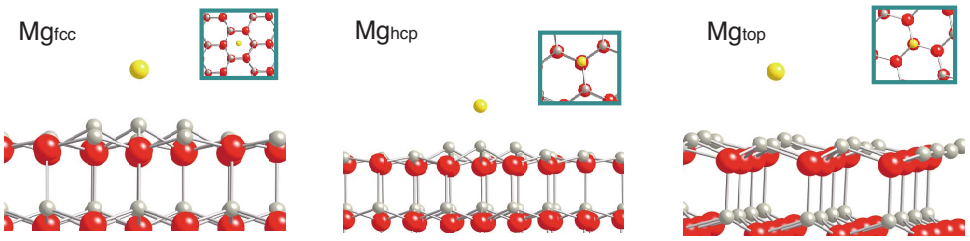

FIG. 3. (Color online) Atomic configuration of the (0001) Zn surface with an adsorbed Mg atom (middle-sized sphere). Top views are also shown in the squares.

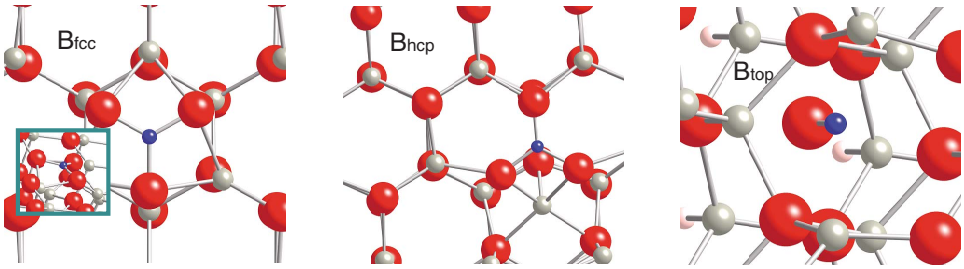

FIG. 4. (Color online) Atomic configuration of the $(000\bar{1})$ O surface with an adsorbed B atom (small sphere). The view from a different angle is shown in the square.

concentration of 6.25%), we obtained the formation energy of +0.32 eV.

III. RESULTS AND DISCUSSION

A. Adsorption on the (0001) Zn surface

The results for the energetics of B and Mg adsorption on the (0001) Zn surface are summarized in Table III. Since the adsorption energies are obtained using the conventional atomic chemical potentials evaluated in their standard reference states, we cannot use those values for a quantitative comparison with experiments but may use them to examine the relative affinities of adatoms. The B atom adsorbed on the fcc site attracts three neighboring Zn atoms and lifts them from the surface (Fig. 2). Similarly, the B atom on the top site attracts one Zn atom from the surface. Both of these processes are unlikely to occur because of high energy cost (Table III). On the other hand, the B atom adsorbed on the hcp site forms a bond with the O atom just below the site with a bond length of 1.31 Å, thereby lowering the adsorption energy down to 0.89 eV. This result clearly indicates that the B atom preferably binds to the O atom rather than the Zn atom even on the (0001) Zn surface. All these adsorption processes of a B atom on the Zn surface are endothermic with respect to the reference atomic chemical potential. In contrast, the adsorption energies of the Mg atom on the fcc and hcp sites are almost the same and their local atomic configurations are also nearly identical (Fig. 3). Each Mg atom has three neighboring Zn atoms within the distance of ~2.75 Å (Table III). The adsorption of Mg on the top site needs about twice higher energy than in the other cases, implying that Mg is hardly adsorbed on the top site. Therefore, the Mg atom, as well as B, on the (0001) Zn surface is unlikely to make strong bonds with the surface atoms and would show a rather diffusive behavior avoiding the route climbing over the Zn atom (top site).

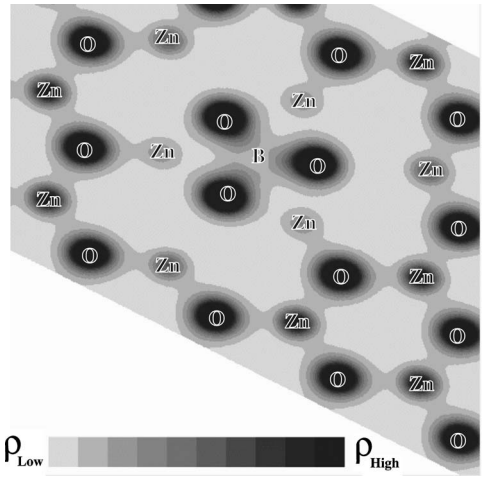

FIG. 5. Valence charge density $\rho(r)$ of the $(000\bar{1})$ O surface with an adatom B on the fcc site. The region of high charge density ρ_{high} is defined as that with $\rho_{high} > 0.2\rho_{max}$, where the ρ_{max} is the maximum charge density. Lower densities are relative to $0.2\rho_{max}$.

B. Adsorption on the $(000\bar{1})$ O surface

The results for the adsorption energetics and geometries of the $(000\bar{1})$ O surface are summarized in Table IV. We find from these results that, in contrast to the Zn surface, this surface shows an extremely reactive behavior for the adsorption of B and Mg atoms.

The B atom on the fcc site forms *triplaner* bonds with the three neighbor O atoms in the distances of ~1.4 Å (Fig. 4). The valence charge density map of the $(000\bar{1})$ surface clearly shows a covalent bonding feature of the triplaner BO_3 binding unit (Fig. 5). Similarly, the B atom on the hcp site forms the same triplaner local atomic configuration by driving out the Zn atom just beneath. Figure 6 schematically shows the triplaner BO_3 binding unit found at these adsorption sites. The adsorption energies of these processes are quite low, and thus all energetically favorable. We note here that the triplaner binding unit is an elemental framework in the B_2O_3

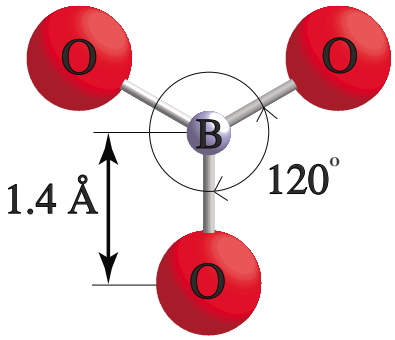

FIG. 6. (Color online) The triplaner BO_3 binding unit found at the fcc and hcp sites on the $(000\bar{1})$ O surface.

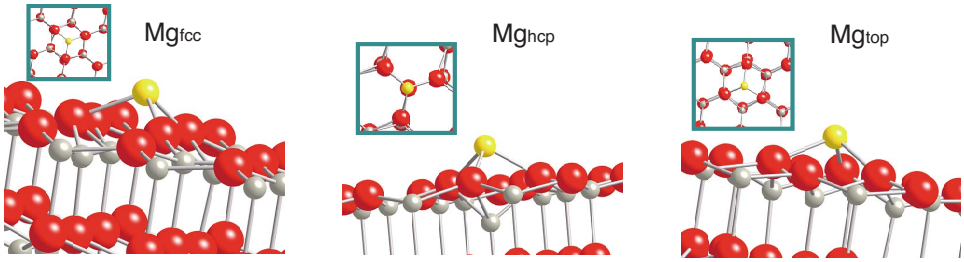

FIG. 7. (Color online) Atomic configuration of the $(000\bar{1})$ O surface adsorbing a Mg atom (middle-sized sphere). Top views are also shown in the squares.

crystal,[33] where the B-O bond length takes the same value of ~1.4 Å. The B atom on the top site binds only to the nearest O atom with the distance of 1.27 Å and the adsorption energy is still negative. Therefore, the adsorption on the top site is exothermic but would be unfavorable because of its relatively high energy cost ($\geqslant$+5.5 eV) compared to the adsorptions on the fcc and hcp sites.

The configurations of Mg atoms adsorbed on the fcc, hcp, and top sites of the O surface show similar local structures. Each of the Mg atoms binds to the three neighbor O atoms at the distance of ~2 Å (Fig. 7). In this case, the O atoms are lifted from the surface and forms a hump of MgO_3 binding unit on the surface. The O-Mg-O bond angle of the binding unit is ~100°. We also find that the Mg atom on the hcp site drives the nearest Zn atom out of the original position below the Mg atom. Hence, it is energetically favorable for the Mg atom to be adsorbed on that site even though it induces deformation of the existing Zn-O bond. We can see a similar local atomic structure in the MgO crystal,[34] where each Mg atom has six neighbor O ligands at the distance of ~2.1 Å and a MgO_6 cage is formed, whereas the Mg atom on the $(000\bar{1})$ O surface has only three neighbor O atoms at shorter distances of 1.97–2.0 Å and their local geometric structure can be viewed as a fraction of a deformed MgO_6 cage in the MgO crystal.

C. Migration energetics on the (0001) Zn surface

We use the well-established climbing nudged-elastic-band (C-NEB) technique[35,36] to explore the energy profiles for the migration process of the adatoms, Mg and B, on the (0001) Zn surface. The calculated energy profile for the Mg migration along the fcc→hcp→top→fcc path is shown in Fig. 8. The energy barrier for the Mg migration from the fcc site to the hcp site is only 0.06 eV. On the other hand, the barrier for the Mg migration along the path climbing over the top site amounts to ~0.5 eV. Therefore, the adsorbed Mg atom would migrate along the path with the lowest energy barrier, fcc→hcp. We note that it is possible for the Mg to migrate throughout the surface area by taking a zigzag route (fcc →hcp→fcc→···), i.e., the Mg atom adsorbed on the (0001) Zn surface shows high mobility characteristics. On the other hand, the energy profile for the B migration on the (0001) Zn surface shows a quite different behavior (Fig. 9). The energy barrier for the B migration for the fcc→hcp route amounts to ~1.4 eV, while it is ~2.4 eV for the reverse route. There is a maximum energy barrier (~3.8 eV) for the B migration along the hcp→top path. The migration of B along the fcc →top path also encounters a high energy cost (~2.8 eV). Therefore, neither of these migration processes would be possible and the B atom adsorbed on the fcc and hcp sites is rather immovable on the (0001) Zn surface and could make bonds with O atoms. We also tried to calculate the energy profile for the Mg and B migrations on the $(000\bar{1})$ O surface but could not obtain any converged result. The tendency of divergence in the C-NEB computation of O surface is understandable since the adatoms form strong bonds with surface O atoms. Any of the intermediate migration point between the specific adsorption sites, and hence the migration path on the O surface, would be indefinite.

Kresse *et al.*[22] have reported that there is a unique stabilization mechanism in the (0001) Zn polar surface, where a certain amount of triangular-shaped defects (pits) are formed to effectively maintain its valency, implying that some oxy-

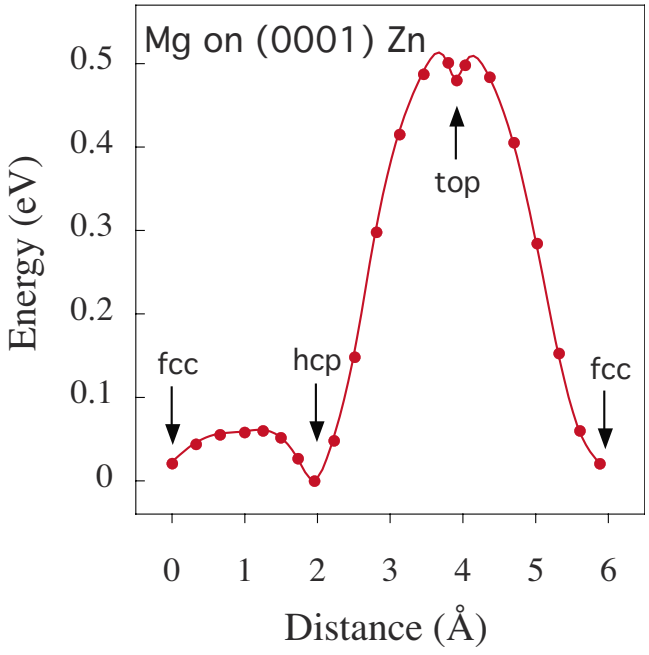

FIG. 8. (Color online) Energy profile for the Mg migration along the fcc→hcp→top→fcc path on the (0001) Zn surface. The energies are measured from the most stable state (hcp site). The horizontal axis is the integrated distance along the optimized migration path. The circles are calculated points and the curve is a guide for the eye.

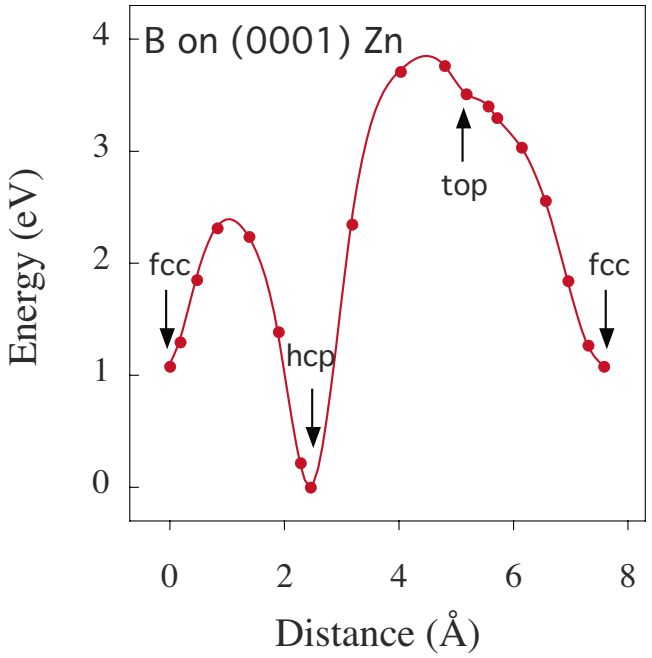

FIG. 9. (Color online) Energy profile for the B migration along the fcc→hcp→top→fcc path on the (0001) Zn surface. The other details are the same as those in Fig. 8.

gen atoms are bare at these intrinsic pits even on the clean (0001) Zn surface. Our results indicate that the bare oxygen atoms, not only on the $(000\bar{1})$ O surface but also on the (0001) Zn surface, easily make bonds with both Mg and B atoms. These reactions will continue until the excess oxygen atoms are exhausted on the surface, and as a result, a thin layer of the reaction products will be left behind in the interface between the epitaxial MgB_2 film and the ZnO substrate.

IV. CONCLUSIONS

A first-principles density-functional PAW method was used to investigate the energetics of Mg and B adsorption on the polar ZnO surfaces, thereby to understand the origin of the peculiar affinities between the epitaxial MgB_2 film and the ZnO substrate. We found that the (0001) Zn surface is relatively inert with respect to the Mg and B adatoms. On that surface, only the B atom on the hcp site forms a bond with the O atom just below the surface Zn layer and its adsorption energy is as low as 0.89 eV, which clearly indicates that the B atom favors to bind to the O atom rather than to the Zn atom even on the (0001) Zn surface. Therefore, both Mg and B atoms are unlikely to make strong bonds with the surface Zn atoms and would show rather diffusive behavior avoiding the route climbing over the Zn atom (top site). On the other hand, the B atoms adsorbed on both the fcc and hcp sites of the $(000\bar{1})$ O surface form the triplaner BO_3 binding units, which can also be found in the B_2O_3 crystal. The Mg atoms adsorbed on the fcc and hcp sites of that surface form a hump of MgO_3 binding unit that can be viewed as a fraction of a MgO_6 cage found in the MgO crystal. These results suggest that the bare oxygen atoms on the ZnO surface easily make bonds with both the Mg and B atoms. These reactions will continue until the excess oxygen atoms are exhausted on the surface and the binding units will be left behind. We note here that a certain amount of triangular-shaped pits are formed even on the clean Zn surface to reduce its valency.[22] In these pits, some oxygen atoms are bared and again make bonds with both Mg and B atoms. As the result, the surface reactions will continue until the excess oxygen atoms are exhausted on both surfaces, leading to the formation of the reaction products that were recently found in the interface between the MgB_2 film and the ZnO substrate. These theoretical results imply that the use of an appropriate buffer layer, which effectively covers the surface oxygen atoms, could suppress the formation of reaction products in the interfaces, or, alternatively, some gettering process for the oxygen at an initial stage of the film formation could work to prevent the formation of reaction products. We need more detailed experimental data for the Mg and B adsorption on the polar ZnO surfaces to verify these implications.

ACKNOWLEDGMENTS

The computations in the present work were performed using the facilities of the Institute for Solid State Physics, University of Tokyo, and of the Information Processing Center of Iwate University. We are grateful to G. Henkelman for providing the C-NEB code. We are also grateful to Y. Komatsu and K. Ohta for assistance in the computations. K.N. thanks M. Baba and Y. Harada for valuable discussions.

*nisidate@iwate-u.ac.jp

[1] J. Nagamatsu, N. Nakagawa, T. Muranaka, Zenitani, and J. Akimitsu, Nature (London) **410**, 63 (2001).
[2] K. Ueda and M. Naito, J. Appl. Phys. **93**, 2113 (2003).
[3] W. Jo, J.-H. Huh, T. Ohnishi, A. Marshall, M. Beasley, and R. Hammond, Appl. Phys. Lett. **80**, 3563 (2002).
[4] M. A. J. van Erven, T. H. Kim, and J. Moodera, Appl. Phys. Lett. **81**, 4982 (2002).
[5] H. Kitaguchi, A. Matsumoto, H. Kumakura, T. Doi, H. Yamamoto, K. Saito, and S. Hata, Appl. Phys. Lett. **85**, 2842 (2004).
[6] G. Grassano *et al.*, Supercond. Sci. Technol. **14**, 762 (2001).
[7] A. Saito, A. Kawakami, H. Shimakage, and Z. Wang, Jpn. J. Appl. Phys., Part 2 **41**, L127 (2002).
[8] K. Tsujimoto, H. Shimakage, Z. Wang, and N. Kaya, Physica C **426-431**, 1464 (2005).
[9] O. Sakata, S. Kimura, M. Tanaka, S. Yata, T. Kato, K. Yamamoto, Y. Yamada, A. Matsushita, and S. Kubo, J. Appl. Phys. **96**, 3580 (2004).
[10] T. Takahashi, Y. Harada, H. Iriuda, M. Kuroha, T. Oba, M. Seki, Y. Nakanishi, J. Echigoya, and M. Yoshizawa, Physica C **445-**

448, 887 (2006).
[11] Y. Harada, T. Takahashi, M. Kuroha, H. Iriuda, Y. Nakanishi, F. Izumida, H. Endo, and M. Yoshizawa, Physica C **445-448**, 884 (2006).
[12] G. Kresse and J. Furthmüller, Phys. Rev. B **54**, 11169 (1996), and references therein.
[13] G. Kresse and D. Joubert, Phys. Rev. B **59**, 1758 (1999).
[14] P. E. Blöchl, Phys. Rev. B **50**, 17953 (1994).
[15] H. J. Monkhorst and J. D. Pack, Phys. Rev. B **13**, 5188 (1976).
[16] J. P. Perdew, K. Burke, and M. Ernzerhof, Phys. Rev. Lett. **77**, 3865 (1996).
[17] J. P. Perdew, K. Burke, and M. Ernzerhof, Phys. Rev. Lett. **78**, 1396 (1997).
[18] D. M. Ceperley and B. J. Alder, Phys. Rev. Lett. **45**, 566 (1980).
[19] J. P. Perdew and A. Zunger, Phys. Rev. B **23**, 5048 (1981).
[20] J. P. Perdew and Y. Wang, Phys. Rev. B **45**, 13244 (1992).
[21] B. Meyer and D. Marx, Phys. Rev. B **69**, 235420 (2004).
[22] G. Kresse, O. Dulub, and U. Diebold, Phys. Rev. B **68**, 245409 (2003).
[23] D. C. Patton, D. V. Porezag, and M. R. Pederson, Phys. Rev. B **55**, 7454 (1997).
[24] J. Albertsson, S. C. Abrahams, and Å. Kvick, Acta Crystallogr., Sect. B: Struct. Sci. **45**, 34 (1989).
[25] Ü. Özgür, Ya. I. Alivov, C. Liu, A. Teke, M. A. Reshchikov, S. Doğan, V. Avrutin, S.-J. Cho, and H. Morkoç, J. Appl. Phys. **98**, 041301 (2005).
[26] A. Nayeb-Hashemi and J. Clark, *Phase Diagrams of Binary Magnesium Alloys*, Monograph Series on Alloy Phase Diagrams (ASM International, Metals Park, OH, 1988).
[27] L. McCarty, J. Kasper, F. Horn, B. Decker, and A. Newkirk, J. Am. Chem. Soc. **80**, 2592 (1958).
[28] K. Reuter and M. Scheffler, Phys. Rev. B **65**, 035406 (2001).
[29] K. Nishidate, T. Sato, Y. Matsukura, M. Baba, M. Hasegawa, and T. Sasaki, Phys. Rev. B **74**, 035210 (2006), and references therein.
[30] *CRC Handbook of Chemistry and Physics*, 82nd ed. (CRC, New York, 2001).
[31] C. G. Van de Walle and J. Neugebauer, J. Appl. Phys. **95**, 3851 (2004).
[32] B. Meyer, Phys. Rev. B **69**, 045416 (2004).
[33] G. E. Gurr, P. W. Montgomery, C. D. Knutson, and B. T. Gorres, Acta Crystallogr., Sect. B: Struct. Crystallogr. Cryst. Chem. **26**, 906 (1970).
[34] C. B. Walker and M. Marezio, Acta Metall. **7**, 769 (1959).
[35] G. Henkelman, B. Uberuaga, and H. Jónsson, J. Chem. Phys. **113**, 9901 (2000).
[36] G. Henkelman and H. Jónsson, J. Chem. Phys. **113**, 9978 (2000).